Payri, R.; De La Morena, J.; Monsalve-Serrano, J.; Pesce, FC.; Vassallo, A. (2019). Impact of counter-bore nozzle on the combustion process and exhaust emissions for light-duty diesel engine application. International Journal of Engine Research. 20(1):46-57. https://doi.org/10.1177/1468087418819250

Impact of counter-bore nozzle on the combustion process and exhaust emissions for light-duty diesel engine application

International Journal of Engine Research 2019, Vol. 20(1) 46–57

R. Payri[1], J. De La Morena[1], J. Monsalve-Serrano[1], F.C. Pesce[2] and A. Vassallo[2]

[1]CMT – Motores Térmicos. Universitat Politècnica de València. Camino de Vera s/n, E-46022 Valencia, Spain.

E-mail: cmt@mot.upv.es
Telephone: +(34) 963 877 650
Fax: +(34) 963 877 659

[2] General Motors Global Propulsion Systems – Torino S.r.l., Corso Castelfidardo 36, 10129 Torino, Italy

Abstract. The present paper describes the main results of an investigation about counter-bore injector nozzle impact on the combustion process in a modern Euro 6 diesel engine. First, hydraulic and spray visualization tests have been performed, showing a potential advantage of such nozzle design in fuel-air mixing efficiency. Then, combustion performance has been assessed on a GM-designed 1.6 liter 4 cylinder engine. The engine has been installed on a dynamometric test bench, and instrumented with an AVL cylinder pressure transducer for heat release rate analysis, as well as HORIBA MEXA gas analyzer for exhaust emissions and AVL 415 Smoke Meter. Engine efficiency and emissions have been analyzed on four different part-load steady state points, representative of NEDC and WLTC certification cycles, and covering engine speeds from 1250 to 2000 rpm and brake mean effective pressure between 2 and 14 bar. Results of indicated analysis show that counter-bore nozzles have significant differences in terms of pilot injection combustion at low load points, which in turn lead to a better ignition and shorter combustion of the main injection. In addition, an improvement of diffusive combustion is observed as load increases. Because of both, fuel consumption is reduced by approximately 1% with respect to a standard nozzle. Finally, an appreciable decrease in engine exhaust emissions has been recorded, especially in terms of PM and HC emissions. This reduction has been linked to the improvement of fuel-air mixing promoted by the counter-bore nozzle previously observed.

1. Introduction

Diesel combustion is highly influenced by the fuel injection system performance. For this reason, significant research effort has been made into analyzing the influence of the injector nozzle geometry into the injector hydraulics [1–3], spray formation [4–7] and combustion [8–10]. In this sense, one of the aspects that can be explored is the shape itself of the nozzle orifices. On an experimental activity, Hong et al. [11] showed that elliptical orifices could help to improve spray atomization, thanks to a more significant cavitation formation inside the nozzle in one of the sides of the ellipse. Molina et al. [12] showed through a computational study that such nozzles had a potential to increase effective velocity and change cavitation patterns inside the nozzle. Taskiran et al. [13] confirmed that divergent shape could help to improve fuel-air mixing and result in shorter lift-off lengths. He et al. [14] compared straight, convergent

and divergent nozzles from the point of view of their hydraulic performance and cavitation formation. Although the divergent shape could be interesting to induce radial velocity at the nozzle outlet and improve mixing, the flow expansion induces a high drop of discharge coefficient. Salvador et al. [15] showed that convergent-divergent shapes can be used to mitigate this issue, enhancing the effective outlet velocity compared to a cylindrical orifice while inducing cavitation in the divergent section, which could help to further improve spray atomization and mixing characteristics. Gasoline fuel injectors currently use counter-bore nozzle orifices [16, 17], which can provide similar mixing advantages as a convergent-divergent shape with a more simple manufacturing process [18].

In the current paper, a counter-bore orifice geometry is investigated for diesel application. Fuel-air mixing characteristics are evaluated by combining liquid and vapor spray visualization tests with a one-dimensional spray model. Then, engine performance and emissions impact are investigated on a fully instrumented 4-cylinder 1.6 liter diesel engine.

As far as the paper structure is concerned, section 2 summarizes all the experimental apparatus used for the investigation, including the hydraulic characterization equipment, the constant-pressure vessel and optical diagnostics for the spray visualization, as well as the engine test bench setup. Section 3 details the numerical approaches used for the 1D spray model, as well as the combustion diagnosis based on the in-cylinder pressure measurement. Section 4 summarizes the main effects of the injector geometry on the nozzle hydraulics. Section 5 analyses the impact of the counter-bore geometry in the fuel-air mixing process. Section 6 evaluates engine combustion results in terms of fuel consumption and emissions. Finally, section 7 provides the most significant conclusions of the study.

2. Experimental setup

2.1 Nozzle geometries

In the current investigation, two kinds of nozzle geometries have been compared. First, a standard microsac nozzle with 340 cm^3/30s flow number and ks-1.5 has been selected as the baseline. Then, a second nozzle with the same flow number definition, but having a counter-bore on the final portion of the orifice, has been manufactured. Figure 1 shows a schematic of the counter-bore orifice design compared with the standard one:

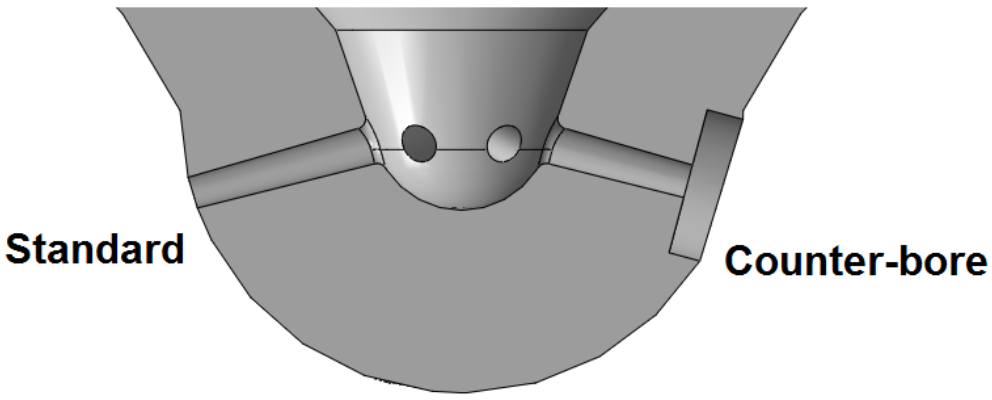

Figure 1: Schematic of standard (left) and counter-bore (right) nozzle orifices

Both nozzles have been mounted on a last-generation solenoid-driven diesel injector, capable of working up to 200 MPa pressure.

2.2. Hydraulic characterization

First of all, both nozzles have been compared from the point of view of their hydraulic performance. For this purpose, two experimental arrangements have been employed.

An EVI injection rate meter (Figure 2) has been used to obtain the instantaneous mass flow rate through the nozzle orifices. This measurement is performed based on Bosch long tube method [19]. In this method, the injection is performed on a fuel-pressurized tube of known diameter, where the instantaneous pressure increase is captured with a piezoelectric pressure transducer. Then, this pressure increase can be correlated to the instantaneous mass flow injected by the nozzle and the fuel properties (in particular the speed of sound). More details about the experimental arrangement and the methodology can be found in [20].

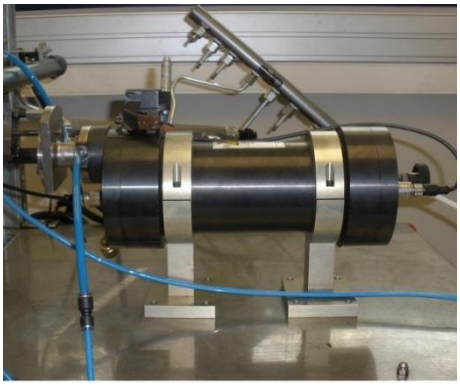

Figure 2: EVI injection rate meter

Additionally, the momentum flux of the emerging spray has been characterized using a dedicated test rig (Figure 3). In this case, the injection is produced on a constant-volume chamber pressurized with nitrogen (up to 8 MPa) at room temperature, emulating similar density conditions as those encountered in the engine combustion chamber during the injection event. A pressure transducer coupled to a measuring target is located perpendicular to one of the nozzle holes at 5mm distance. When the injection starts, the spray impact force on the target is transmitted to the sensor and captured by the acquisition system. Once the setup is properly calibrated, this impact force can be converted into the spray momentum flux. More details about this methodology can be found in [3].

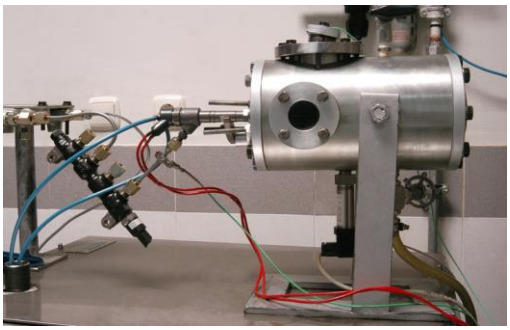

Figure 3: Spray momentum flux test rig

The combination of both injection rate and momentum flux measurements can be used to obtain information about the effective outlet area (A_{eff}) and effective outlet velocity (u_{eff}) of the nozzle. Once the injector needle is sufficiently high and the injection reaches quasi-steady state conditions, the mass flow ($\dot{m}_f$) and momentum flux ($\dot{M}_f$) can be defined as:

$$\dot{m}_f = \rho_f A_{eff} u_{eff} = C_d \rho_f A_o u_o \quad [1]$$
$$\dot{M}_f = \rho_f A_{eff} u_{eff}^2 = C_M \rho_f A_o u_o^2 \quad [2]$$

Consequently, the effective area and velocity can be calculated as:

$$u_{eff} = \frac{\dot{M}_f}{\dot{m}_f} \quad [3]$$

$$A_{eff} = \frac{\dot{m}_f}{\rho_f u_{eff}} \quad [4]$$

2.3. Spray vessel

Spray visualization tests are performed on a high-pressure and high-temperature vessel with up to three optical accesses (Figure 4). The vessel operates at constant pressure conditions (up to 16 MPa). A set of resistances heats the incoming gas flow up to a maximum value of approximately 900 K. The working gas can be nitrogen (working on inert conditions), air or a combination of both for synthetic Exhaust Gas Recirculation (EGR) operation.

Figure 4: spray vessel

2.3.1 Mie-scattering (liquid spray visualization)

Mie-scattering technique is used to visualize the evaporative liquid spray (Figure 5). In this technique, two continuous light sources are placed in the lateral windows of the spray vessel. The light impacting on the spray droplets scatters, reaching the sensor of a high-speed Photron Fastcam SA-X2 CCD camera placed in the frontal window, parallel to the injector axis. The camera is equipped with a Nikkor 50mm f/2 lens. The camera operates at 30000 frames per

second, producing images every 33 µs during the injection event. The resolution of each image is 640x640 pixels, reaching 6.7 pixels/mm. Exposure time is set to 6.25 µs.

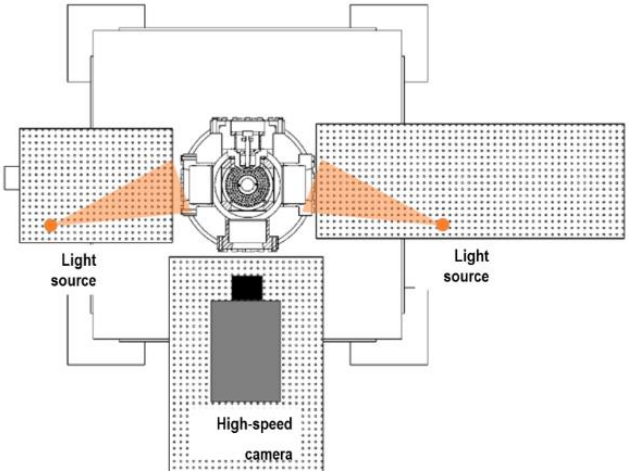

Figure 5: Mie-scattering (liquid spray) optical arrangement

2.3.2 Shadowgraphy

In the case of the vapour spray visualization, shadowgraphy technique is used (Figure 6). In this arrangement, a punctual light source is directed using a beam splitter to a collimated lens, producing a set of parallel light beams arriving to the vessel and being reflected on a high-temperature metal mirror. When the beams reach the spray in either way, its different density results in a change of the refractive index, deviating them. The beams not passing through the fuel spray are not deviated and arrive unaltered to the high-speed camera sensor, producing a negative image of the sprays. An adjustable Fourier diaphragm is placed upstream the camera to cancel reflections coming from other components. The same CCD camera and configuration as already detailed for the Mie-scattering technique is used.

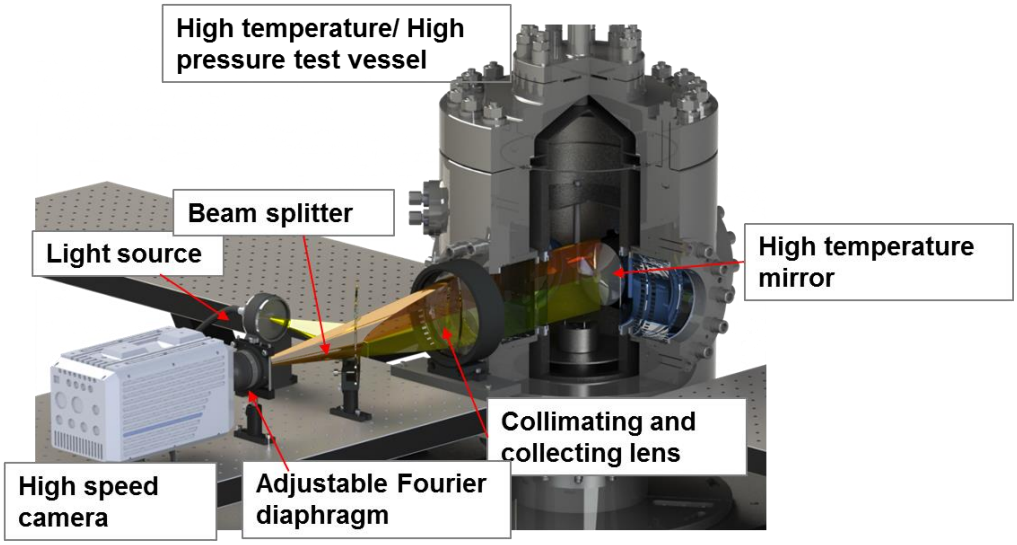

Figure 6: Shadowgraphy (vapor spray) optical arrangement

2.4 Engine test bench

For the current investigation, a GM 4-cylinder 1.6 liter Euro 6 diesel engine has been employed. The main engine characteristics are summarized in Table 1.

Table 1: Main engine dimensions and systems

Parameter	**Unit**	**Value**
Compression ratio	-	16:1
Bore	mm	79.7
Stroke	mm	80.1
Connecting rod length	mm	140
Pin offset	mm	0.5
Swirl ratio	-	1.9-3.6
Fuel injection system	-	Solenoid 3rd generation, 200 MPa
EGR system	-	Low-pressure + high-pressure
Turbocharger	-	Single-state VGT

Figure 7 shows a schematic of the engine test bench used for the study, including the locations for the different pressure sensors and thermocouples. AVL GH14P piezoelectric pressure transducer has been introduced into the glow-plug location on one of the central cylinder to acquire instantaneous in-cylinder pressure and perform heat release rate analysis. Exhaust emissions were obtained at the turbine outlet by means of a Horiba MEXA 7100 system and an AVL 415 Smoke meter. Fuel consumption was measured using an AVL 733S fuel gravimetric balance. A dynamometric brake controlled with AVL PUMA is used to control the engine speed and acquire the engine torque. The Electronic Control Unit (ECU) of the engine is controlled using ETAS INCA v7.1.

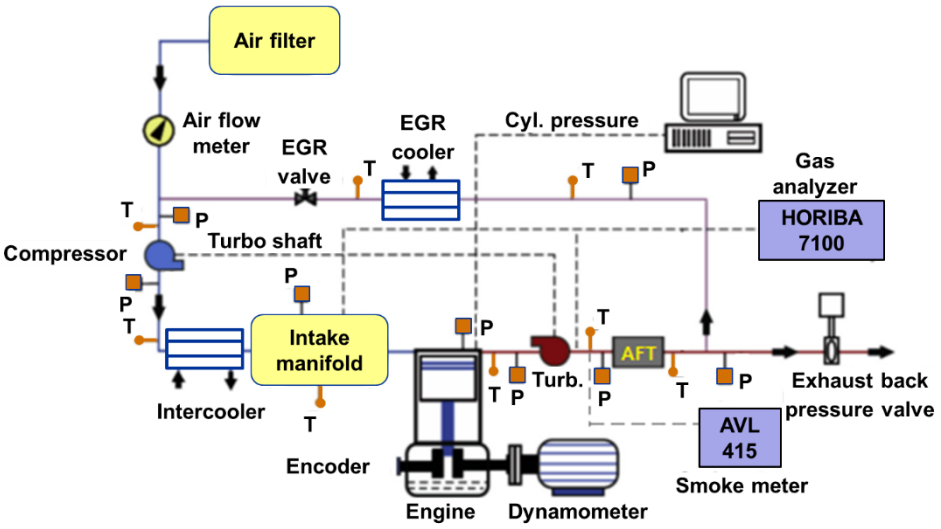

Figure 7: engine test bench configuration

Engine operation has been evaluated in four steady-state points in terms of engine speed (rpm) and Brake Mean Effective Pressure (MPa): 1250x0.2, 2000x0.5, 2000x0.8 and 1500x1.4. These points were selected due to their high impact on NEDC and WLTP certification cycles for the related applications of the engine. For each of these points, an EGR sweep has been performed for three different calibration strategies: the baseline, one with increased electrical separation between pilot and main injection (called high-DT), and a final one with increased rail pressure (called high-PRail). The EGR range for the sweep has been tailored for each key-point with the objective of achieving an absolute EGR rate variation of ±10%, but limiting smoke emissions to a maximum of 4 FSN.

Finally, table 2 summarizes the main characteristics of the diesel fuel used for the study.

Table 2: fuel properties

Parameter	**Unit**	**Value**
Cetane number	[−]	51.6
Viscosity at 40 °C	[mm^2/s]	2.46
Density at 15 °C	[kg/dm^3]	0.843
Lower heating value	[MJ/kg]	42.055
Sulfur content	[ppm]	6.6
Biodiesel content	[%]	5

3. Numerical approach

3.1 One-dimensional spray model

In the current model, the spray is assumed to be injected into a quiescent air volume, which is large enough so that flow evolution does not modify air conditions far away from the nozzle. These conditions are similar to those existing on the previously defined spray vessel. Additionally, the following hypotheses are made:

1. Symmetry on the spray axis, i.e., no air swirl.
2. A fully developed turbulent flow is assumed, which means that self-similar radial profiles can be defined for the conserved variables. In the present approach, a radial Gaussian profile is assumed, so that:

$$\frac{u(x,r)}{u_{cl}(x)} = \left[\frac{f(x,r)}{f_{cl}(x)}\right]^{1/Sc} = exp\left[-k\left(\frac{r}{x}\right)^2\right] \quad [5]$$

where $u_{cl}(x)$ and $f_{cl}(x)$ are values on the spray axis of the axial component of the velocity vector and mixture fraction, respectively, k is a constant, and *Sc* is the turbulent Schmidt number.

3. Linked to the previous assumption, the spray cone angle is defined as the location where the axial velocity is ζ = 1% of the value on the spray axis, so that:

$$k = \frac{ln(1/\zeta)}{tan^2(\theta/2)} \quad [6]$$

4. The turbulent Lewis number is assumed to be equal to 1. Consequently, the local enthalpy, for which no conservation equation is solved, can be expressed as:

$$h(x,r,t) = h_{a,\infty} + f(x,r,t)\left(h_{f,0} - h_{a,\infty}\right) \quad [7]$$

where $f(x, r, t)$ is the local mixture fraction value and $h_{f,0}$ and $h_{a,\infty}$ are the enthalpy of pure fuel (nozzle outlet conditions) and pure air (far away from the nozzle), respectively. This relationship is independent of the general flow calculations, so that state relationships can be calculated a priori, as will be shown below.

5. The pressure is assumed to be constant all over the spray.
6. A locally homogeneous flow is assumed, i.e., local equilibrium exists both in thermal and velocity conditions. This allows for the consideration of the spray as a single-fluid jet.

This leads to the following formulation of the conservation equations for the spray momentum and fuel mass:

$$I(x_i,t) - I(x_{i+1},t) = \frac{d}{dx}\int \rho u dV \quad [8]$$

$$M_f(x_i,t) - M_f(x_{i+1},t) = \frac{d}{dx}\int \rho f dV \quad [9]$$

These equations are solved at each axial position of the spray, obtaining the values of the fuel mass fraction (*f*) and velocity (*u*) at the spray centerline. Eventually, once *f* is obtained at one location, local temperature, density, and composition can also be calculated from state relationships. In the current study, the experimental input data regarding the instantaneous mass flow rate and momentum flux at the nozzle outlet, obtained through the methodology detailed in section 2.2, is fed into the model to compute the transient spray evolution.

More details about the model formulation and calculation methodology can be found in [21, 22].

3.2 In-cylinder pressure diagnostics

In-cylinder pressure evolution can be used to estimate the combustion characteristics in terms of instantaneous Heat Release Rate (HRR) evolution. For this purpose, 1st law of thermodynamics can be applied to the engine operation according to the following formulation:

$$dHR = -m_c\, du_c - pdV - dQ_w + \left(h_{fl} - u_f\right)dm_{fg} - RTdm_{bb}\ [10]$$

Where m_c is the trapped mass in the cylinder, u_c the internal energy of the gas, Q_w the heat transfer to the walls, h_{fl} and u_f the enthalpy and internal energy of the fuel (in liquid and gas phase, respectively), m_{fg} the evaporated fuel mass and m_{bb} the blow-by mass.

In order to estimate heat transfer losses, Woschni model is adjusted according to the following formulation:

$$h_w = 1.3 \cdot 10^{-2} D^{-0.2} p^{0.8} T^{-0.53} \left(C_{w1} c_m + C_{w2} c_u + C_2 \frac{V \cdot T_{IVC}}{p_{IVC} \cdot V_{IVC}} (p - p_0) \right)^{0.8} [11]$$

Being h_w the heat transfer coefficient, D the cylinder bore, C_{w1}, C_{w2} and C_2 constants adjusted according to motoring tests, c_m the mean piston velocity, c_u the tangential velocity (depending on the engine swirl) and subindex *IVC* represents conditions at Intake Valve Closure.

Finally, a mechanical deformations model is included to take into account the changes of the in-cylinder volume depending on pressure and inertia terms:

$$\Delta V = \Delta V_p + \Delta V_i = K_{def} \frac{\pi D^2}{2} \frac{p}{E_s} \left(\frac{D}{d_b}\right)^2 L_0 + K_{def} \frac{m \cdot a}{E_s} \left(\frac{D}{d_b}\right)^2 L_0 [12]$$

Where K_{def} is a constant, E_s is the Young modulus of the material, d_b is the piston bowl diameter, L_0 is the geometrical length of the slider-crank mechanism (including crankshaft, connecting rod and piston), m is the piston mass and a is the piston acceleration.

More details about the heat release rate calculation and constants adjustment methodologies can be found in [23].

4. Hydraulic characterization

As stated into the introduction, one of the potential effects of the usage of counter-bore orifices could be a potential decrease of the nozzle permeability due to the expansion in this large diameter portion. This information can be directly extracted from the injection rate measurements in terms of the discharge coefficient multiplied by the nozzle orifice area (Figure 8). As it can be seen, the results show that the counter-bore nozzle is capable to increase its nozzle compared to the standard, even though the differences between both are small. This behavior may be due to lower friction losses inside the orifice, related to its lower length.

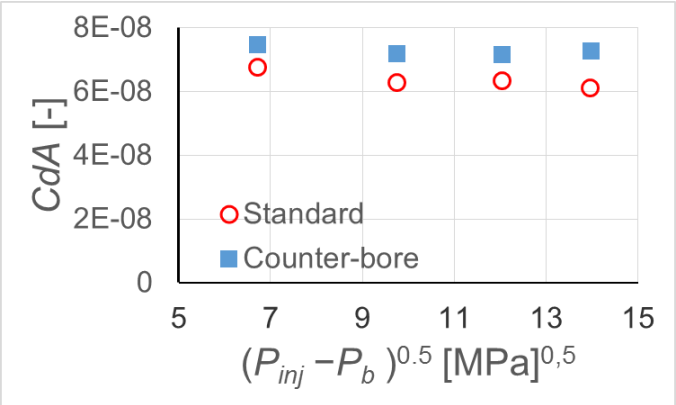

Figure 8: Nozzle permeability (CdA) vs. the square root of the pressure drop

Additionally, the information from injection rate and momentum flux can be combined to obtain the nozzle effective outlet velocity and diameter, as detailed in section 2.2. This information is available in Figure 9. The main difference observed is regarding the effective diameter, which seems to be significantly larger for the counter-bore nozzle even though the nozzles had been defined with the same flow number. In terms of effective velocity, no significant difference is achieved.

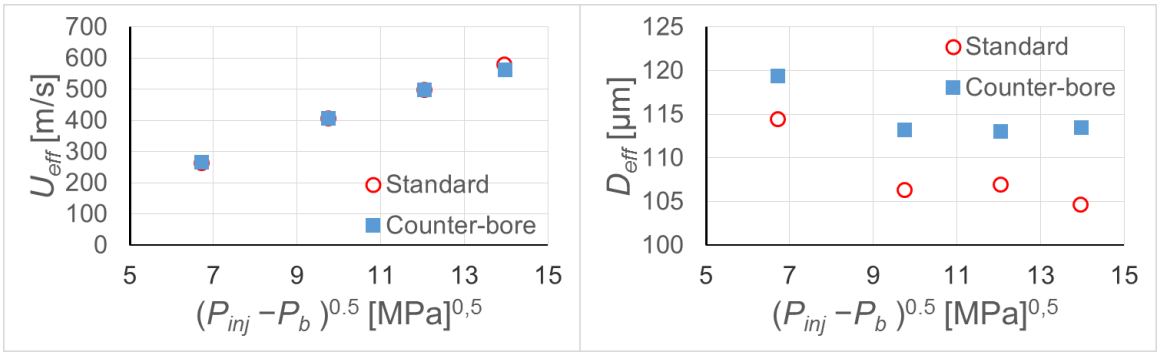

Figure 9: Nozzle effective velocity (left) and diameter (right) vs. the square root of the pressure drop

5. Mixing evaluation

Figure 10 shows the results in terms of vapor and liquid spray penetration and angle for an operating point of injection pressure 100 MPa, chamber temperature 800K and chamber density 21.5 kg/m^3. Standard nozzle is represented by a red line, while counter-bore nozzle is depicted in a blue line. For each set of data, dashed lines representing the upper and lower limit of the uncertainty band (represented by the average value plus or minus the measured standard deviation) are also included. As it can be seen, small differences are appreciable between the nozzles. Counter-bore nozzle is characterized by slightly longer spray penetration and liquid length. Regarding the spray angle, some benefit is seen for this counter-bore nozzle, especially at the beginning of the injection event. Nevertheless, it has to be noted that differences in spray angle are close to the magnitude of the uncertainty band, so they are not very significant.

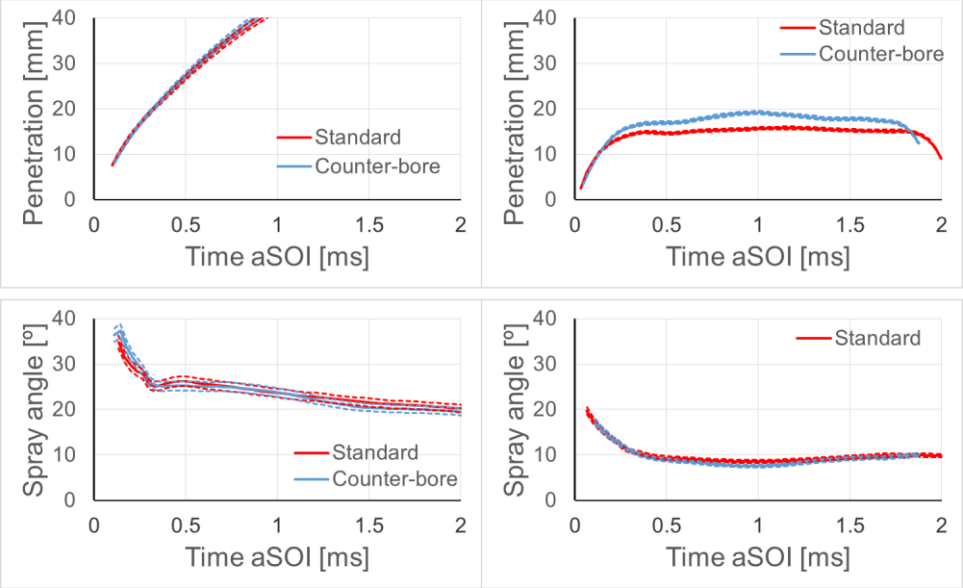

Figure 10: Vapor (left) and liquid (right) spray visualization results for P_i=100 MPa, T=800 K and ρ_a=21.5 kg/m^3

The small differences seen in spray penetration are partially due to the fact that the counter-bore nozzle has a higher effective diameter, as previously identified on the nozzles' hydraulic characterization. Thus, a better evaluation of fuel-air mixing can be provided by defining a fuel-based spray density, which is calculated as the ratio between the fuel injected quantity at a certain time step and the spray volume estimated from the vapor spray visualization contours. This magnitude is presented in Figure 11 in a ratio between the values obtained for the counter-bore and standard nozzle. As it can be observed, for injection pressures equal to or lower than 100 MPa, the fuel-based spray density of the counter-bore nozzle is lower than that of the standard one after an initial transient, since the ratio is lower than 1. This implies that, at similar spray volume, the counter-bore nozzle includes lower fuel quantity and, consequently, higher air entrainment.

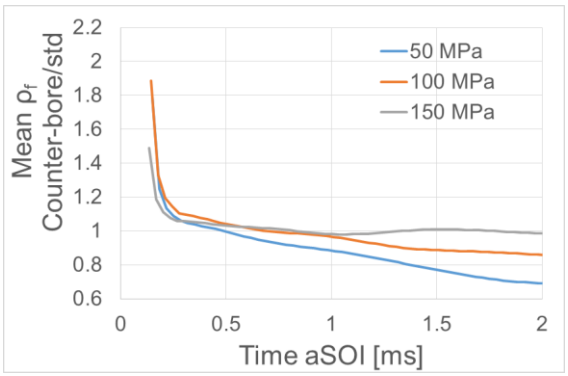

Figure 11: ratio of fuel-based spray density

This analysis is complemented with the results from the 1D spray model, previously validated [24]. These results are depicted in Figure 12. As it can be seen, the counter-bore nozzle (blue line) shows significantly higher air entrainment than the standard (red line), resulting in a longer portion of the fuel mass distributed in low equivalence ratio values (below 1.5). As a consequence, increase air entrainment achieved for the counter-bore design offers the potential for

a soot reduction in engine operation. Nevertheless, more detailed analysis through 3D-CFD simulations would be required for a more deep understanding of the fuel-air mixing characteristics provided by the counter-bore design compared to the standard.

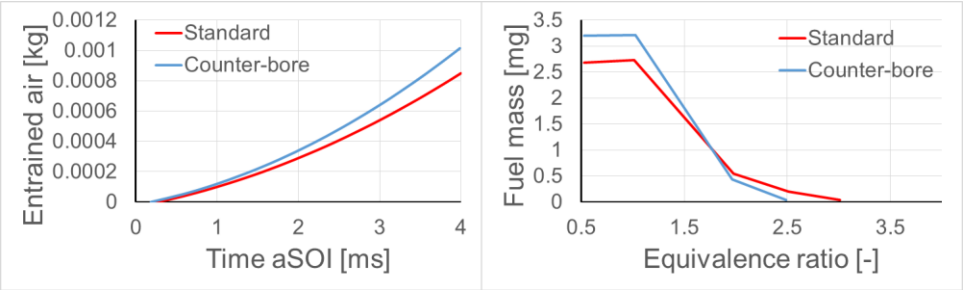

Figure 12: 1D spray model results

6. Engine combustion

6.1 In-cylinder pressure analysis

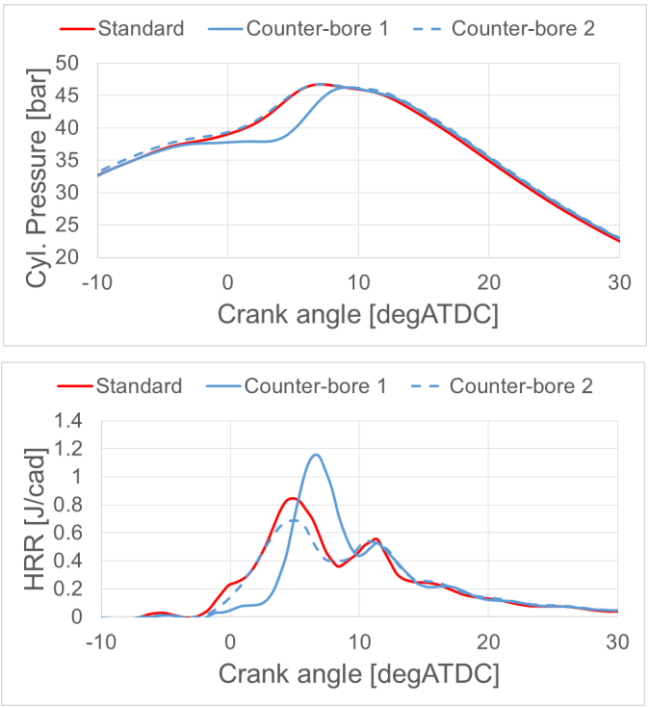

Figure 13: in-cylinder pressure and heat release rate for 1250x0.2

Figure 13 shows the results of the in-cylinder pressure and heat release rate analysis for an operating point of 1250 rpm and 0.2 MPa BMEP. In this graph, the standard nozzle is represented by the red continuous line with the baseline calibration, characterized by two pilot injections, being the second pilot close-coupled to the main, and a post-injection. For the counter-bore nozzle, two different calibrations are compared. First, the same baseline calibration is depicted in continuous blue line (Counter-bore 1). Compared to the standard one, it is clearly seen that the burning efficiency of the pilot masses is very low, resulting in a larger ignition delay for the main injection and a more significant premixed combustion phase. This result can be analyzed looking back at the fuel-based spray density shown in Figure 11. In this figure, it is possible to see that during the initial stages of the injection event, the fuel-based density of the counter-bore nozzle is significantly higher, which are characteristic of the pilot injections operation. Thus, the poorer mixing of these pilot injections can result in less efficient combustion, and explain the results obtained in the engine.

In order to correct this undesired behavior, a new calibration aimed at providing a similar in-cylinder pressure as the standard injector has been searched. To do so, the pilot masses have been increased from 1.3 to 1.8 mm^3/st. This result is plotted in a dashed blue line in the figure (labelled Counter-bore 2). Although this calibration is capable to accurately reproduce the in-cylinder pressure evolution, it is still noticeable in the heat release rate that the energy released by the pilot injections is lower than for the standard nozzle. Similar behavior was also found for 2000x0.5 keypoint.

Figure 14 shows a similar analysis for the 1500x1.4 operating point. In this case, the baseline calibration provided similar pilot burning efficiency and premixed heat release rate peaks for both nozzles, so no calibration correction was necessary. Nevertheless, the counter-bore nozzle provided higher heat release rate during the mixing-controlled combustion phase, which could be seen as an indicator or a better air utilization induced by enhanced mixing. Similar results were also seen for the other mid-load point (2000x0.8).

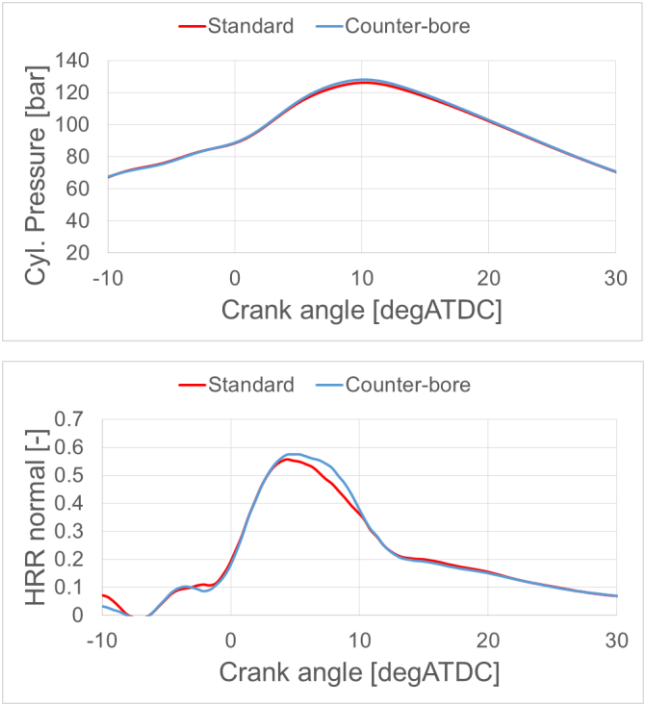

Figure 14: in-cylinder pressure and heat release rate for 1500x1.4

6.2 Engine performance and emissions

Engine operation has been assessed by a set of sweeps of EGR rate around the baseline calibration condition. Each of these sweeps has been performed for both nozzles using three calibration strategies:

1) Baseline calibration. In the case of the counter-bore nozzle, the modified calibration with increased pilot masses was selected as the baseline, so that the comparison between injectors was done at almost equal heat release rate characteristics.
2) High dwell time (DT): increase of 0.2 ms in the electrical dwell time between the closest pilot and the main injections
3) High injection pressure (PRail): increase of ~15 MPa in the rail pressure.

For each of these variations, engine performance has been evaluated in terms of fuel consumption, combustion noise and exhaust emissions. Additionally, a complete Design of Experiments (DOE) with variations of all calibration parameters was completed for one of the operating points (in particular, 2000 rpm x 0.8 MPa BMEP). The variations for each parameter of this DOE were selected to achieve low-NOx values.

Figure 15 shows the results in terms of fuel consumption and combustion noise for two operating points: 2000x0.5 and 2000x0.8. Generally, the 2000x0.5 points shows some benefit in terms of fuel consumption for the counter-bore nozzle, while this benefit is more limited in the case of the 2000x0.8 point. This advantage comes mostly from a reduction in heat transfer losses, plus a slight reduction in combustion duration. Combustion noise is equivalent for the baseline calibration, which was optimized for this parameter, while the behavior induced by the calibration change for each operating keypoint was quite different. For the 2000x0.5, an increase of either the injection pressure or the dwell time results in an increase of the noise. It has to be noted that the pilot burning on the counter-bore nozzle for this operating point was not robust, which was compensated by increasing the pilot masses on the baseline calibration. This compensation effect is probably not optimized once the calibration strategy changes, resulting in a combustion noise deterioration. For the 2000x0.8, were no pilot mass compensation was necessary, the counter-bore nozzle showed and advantage in terms of combustion noise when changing the calibration characteristics.

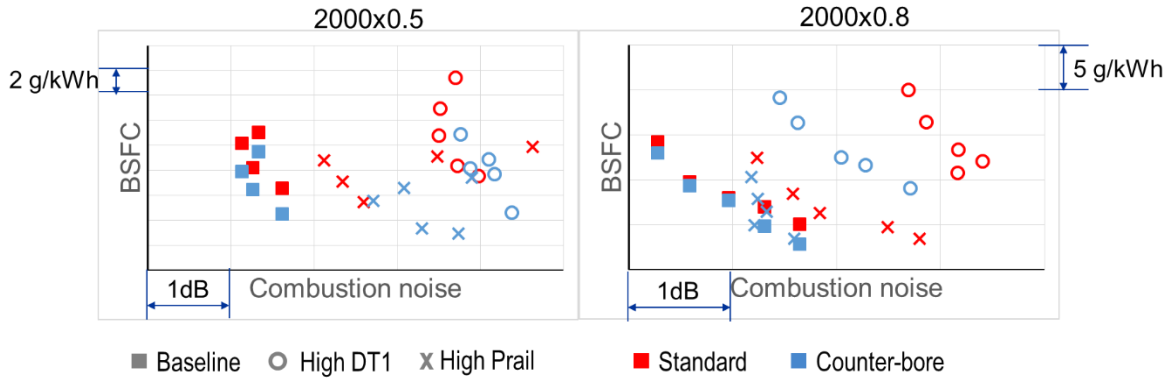

Figure 15: BSFC and combustion noise results for 2000x0.5 and 2000x0.8

Figure 16 analyzes instead smoke and NOx exhaust emissions, which are the most significant for diesel engine combustion. In the 2000x0.5, the counter-bore nozzles provide some benefit in smoke-NOx tradeoff values for all the tests performed. This is consistent with the better mixing efficiency previously analyzed. Comparing the different calibration strategies, it can be seen that the smoke-NOx reduction achieved with the counter-bore nozzle is greater when combining high levels of EGR (low NOx values) and baseline calibration. When increasing load (2000x0.8), the smoke emissions benefit appears only for the standard and high PRail calibrations combined with high EGR rates (low NOx), while the emissions characteristics are roughly equivalent otherwise.

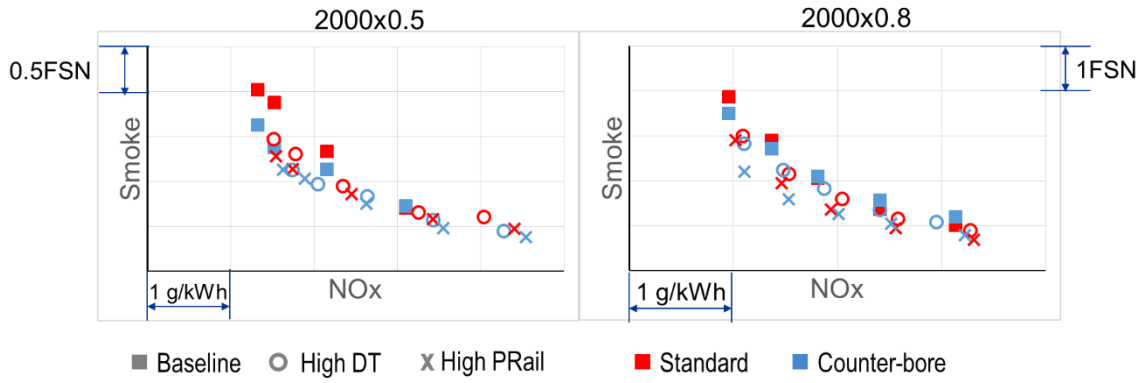

Figure 16: Smoke and NOx emissions results for 2000x0.5 and 2000x0.8

Finally, CO and HC emissions are also evaluated in Figure 17. In the 2000x0.5, some deterioration is observed for the high DT calibration, while for the rest there is generally a benefit in HC. In the case of 2000x0.8, CO emissions are approximately equivalent, while the advantage in HC is maintained.

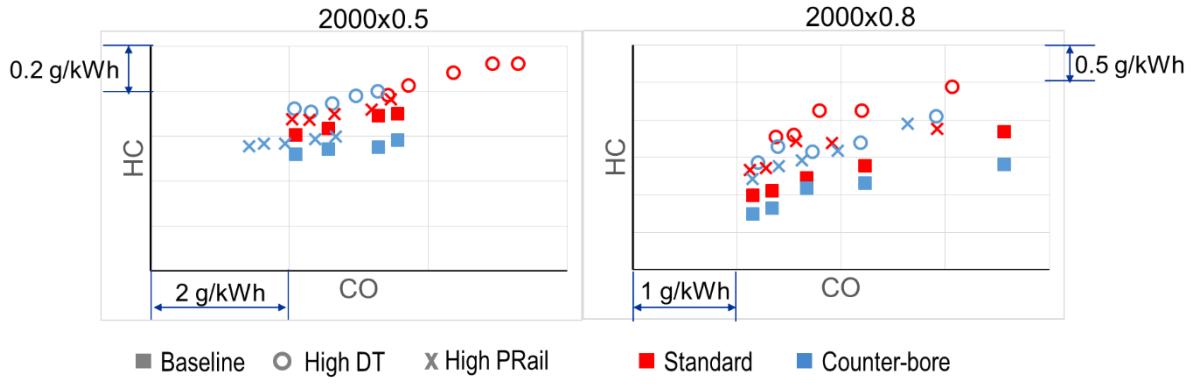

Figure 17: HC and CO emissions results for 2000x5 and 2000x8

Finally, Figure 18 shows the results from the complete DOE performed on the 2000 rpm x 0.8 MPa BMEP condition. As it can be seen, the full variation confirms the previous trends observed in terms of BSFC reduction (~2-3 g/kWh) and smoke reduction (~1FSN) for the same NOx emissions level for these conditions. Additionally, in this case some CO advantage has been observed.

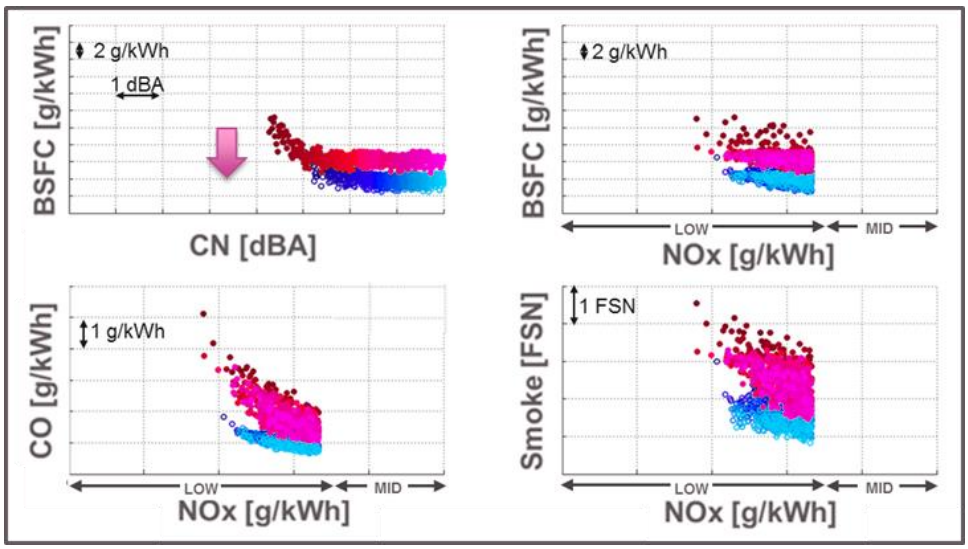

Figure 18: results from full DOE at 2000x0.8 operating point. Red: standard nozzle, Blue: counterbore nozzle.

7. Conclusions

In the current study, an investigation of the effect of using counter-bore nozzle orifices in diesel spray and combustion characteristics has been performed. For this purpose, hydraulic characterization and inert spray visualization results have been combined with engine combustion tests.

The hydraulic characterization shows that the counter-bore orifices had no negative impact on the nozzle permeability. Actually, a small advantage in this sense is noticed, probably due to the lower orifice length and related viscous friction losses. Outlet velocity was also equivalent, while the effective diameter was higher for the counter-bore.

From the spray visualization tests, the following conclusions can be drawn:

- Liquid and vapor spray penetration are slightly larger for the counter-bore nozzle, mostly due to an increase of the orifices effective diameter previously evaluated.
- Vapor spray angle is larger for the counter-bore nozzle during the spray initial stages. As the spray develops, both nozzles provide equivalent results.
- Fuel based spray density has been calculated as the instantaneous ratio between the spray volume obtained from the vapor visualization data and the cumulated injected quantity from injection rate measurements. This parameter shows better fuel-air mixing for the counter-bore nozzle for injection pressures lower than 150 MPa.

- A one-dimensional spray model previously validated was used to obtain further information regarding fuel-air mixing efficiency, showing better performance in both entrained air and equivalence ratio distribution for the counter-bore nozzle.

In the case of the engine characterization, main comparison is performed in terms of heat release rate characteristics, fuel consumption, combustion noise and exhaust emissions. The main conclusions are:

- In the low load range (1250x0.2 and 2000x0.5), different mixing characteristics during the initial injection stages results in a deterioration of the pilot burning efficiency for the counter-bore nozzle. Thus, an increased of the premixed combustion phase is achieved if constant pilot fueling is applied. An increase of around 0.5 mg/st in these pilots masses is necessary to achieve similar heat release rate characteristics, even if some reduction in pilot combustion is still present.
- In the mid-to-high load range (2000x0.8 and 1500x1.4), pilot burning is no longer an issue, and some benefit appears for the counter-bore nozzle in terms of diffusion (mixing-controlled) heat release rate gradient.
- Fuel consumption is generally lower for the counter-bore nozzle at low loads, induced by a combination of lower heat transfer losses and shorter combustion duration. For higher loads, fuel consumption outcome is equivalent.
- For the combustion noise, different behavior appears depending on the engine load. At low loads, sensitivity of the pilot burning for the counter-bore nozzle tends to produce a deterioration of this parameter when increasing either dwell time or injection pressure. On the contrary, better results in combustion noise are achieved for the counter-bore nozzle at higher loads.
- Better fuel-air mixing is translated into a better smoke-NOx tradeoff for the counter-bore nozzle. This benefit tends to reduce when using low EGR rates or large electrical dwell times.
- CO emissions are generally similar, while some reduction in HC is seen for the counter-bore nozzle.

Acknowledgments

The authors would like to thank General Motors Global Propulsion Systems – Torino S.r.l. for sponsoring the current work.

References

[1] Kastengren AL, Tilocco FZ, Powell CF, et al. Engine Combustion Network (ECN): Measurements of Nozzle Geometry and Hydraulic Behavior. *At Sprays* 2012; 22: 1011–1052.

[2] Payri R, Viera JP, Gopalakrishnan V, et al. The effect of nozzle geometry over internal flow and spray formation for three different fuels. *Fuel* 2016; 183: 20–33.

[3] Postrioti L, Malaguti S, Bosi M, et al. Experimental and numerical characterization of a direct solenoid actuation injector for Diesel engine applications. *Fuel* 2014; 118: 316–328.

[4] Payri R, Gimeno J, De la Morena J, et al. Study of new prototype pintle injectors for diesel engine. *Energy Convers Manag* 2016; 122: 419–427.

[5] Payri R, Bracho G, Marti-Aldaravi P, et al. Near field visualization of diesel spray for different nozzle inclination angles in non-vaporizing conditions. *At Sprays* 2017; 27: 251–267.

[6] Shi J, Aguado PL, Dober G, et al. Using LES and x - ray imaging to understand the influence of injection hole geometry on Diesel spray formation. *THIESEL 2016 Conf Thermo- Fluid Dyn Process Diesel EnginesConference Thermo Fluid Dyn* 2016; 1–21.

[7] Li T, Moon S, Sato K, et al. A comprehensive study on the factors affecting near-nozzle spray dynamics of multi-hole GDI injectors. *Fuel* 2017; 190: 292–302.

[8] Yu W, Yang W, Zhao F. Investigation of internal nozzle flow, spray and combustion characteristics fueled with diesel, gasoline and wide distillation fuel (WDF) based on a piezoelectric injector and a direct injection compression ignition engine. *Appl Therm Eng* 2017; 114: 905–920.

[9] Payri R, Viera JP, Gopalakrishnan V, et al. The effect of nozzle geometry over ignition delay and flame lift-off of reacting direct-injection sprays for three different fuels. *Fuel* 2017; 199: 76–90.

[10] Yao C, Geng P, Yin Z, et al. Impacts of nozzle geometry on spray combustion of high pressure common rail injectors in a constant volume combustion chamber. *Fuel* 2016; 179: 235–245.

[11] Hong JG, Ku KW, Kim SR, et al. Effect of cavitation in circular nozzle and elliptical nozzles on the spray characteristic. *At Sprays* 2010; 20: 877–886.

[12] Molina S, Salvador FJ, Carreres M, et al. A computational investigation on the influence of the use of elliptical orifices on the inner nozzle flow and cavitation development in diesel injector nozzles. *Energy Convers Manag* 2014; 79: 114–127.

[13] Taskiran OO, Ergeneman M. Effect of nozzle dimensions and fuel type on flame lift-off length. *Fuel* 2014; 115: 833–840.

[14] He Z, Guo G, Tao X, et al. Study of the effect of nozzle hole shape on internal flow and spray characteristics. *Int Commun Heat Mass Transf* 2016; 71: 1–8.

[15] Salvador FJ, de la Morena J, Carreres M, et al. Numerical analysis of flow characteristics in diesel injector nozzles with convergent-divergent orifices. *Proc Inst Mech Eng Part D J Automob Eng* 2017; 231: 1935–1944.

[16] Baldwin ET, Grover RO, Parrish SE, et al. String flash-boiling in gasoline direct injection simulations with transient needle motion. *Int J Multiph Flow* 2016; 87: 90–101.

[17] Tu P, Cao L, Xu H, et al. Numerical Investigation of GDI Injector Nozzle Geometry on Spray Characteristics. *SAE Tech Pap 2015-01-1906*. Epub ahead of print 2015. DOI: 10.4271/2015-01-1906.

[18] Serizawa K, Ueda D, Mikami N, et al. Realizing Robust Combustion with High Response Diesel Injector with Controlled Diffusive Spray Nozzle and Closed Loop Injection Control. Epub ahead of print 2018. DOI: 10.4271/2017-01-0845.Copyright.

[19] Bosch W. The Fuel Rate Indicator: A New Measuring Instrument for Display of the Characteristics of Individual Injection. *SAE Tech Pap 660749*. Epub ahead of print 1966. DOI: 10.4271/660749.

[20] Payri R, Salvador FJ, Gimeno J, et al. A new methodology for correcting the signal cumulative phenomenon on injection rate measurements. *Exp Tech* 2008; 32: 46–49.

[21] Desantes JM, Pastor JV, Garcia-Oliver JM, et al. A 1D model for the description of mixing-controlled reacting diesel sprays. *Combust Flame* 2009; 156: 234–249.

[22] Pastor JV, Lopez JJ, Garcia-Oliver JM, et al. A 1D model for the description of mixing-controlled inert diesel sprays. *Fuel* 2008; 87: 2871–2885.

[23] Payri F, Molina S, Martín J, et al. Influence of measurement errors and estimated parameters on combustion diagnosis. *Appl Therm Eng* 2006; 26: 226–236.

[24] Payri R, De La Morena J, Monsalve-Serrano J, et al. Analysis of spray characteristics on a counter-bore fuel injector nozzle for diesel engine application. In: *SIA Diesel Powertrain International Conference*. 2018, pp. 1–8.